[Research Paper] 대한금속 · 재료학회지 (*Korean J. Met. Mater.*), Vol. 59, No. 12 (2021) pp.904-910
DOI: 10.3365/KJMM.2021.59.12.904

Synthesis of $Nb_{0.8}Hf_{0.2}FeSb_{0.98}Sn_{0.02}$ and $Hf_{0.25}Zr_{0.25}Ti_{0.5}NiSn_{0.98}Sb_{0.02}$ Half-Heusler Materials and Fabrication of Thermoelectric Generators

Sung-Jae Joo*, Ji-Hee Son, JeongIn Jang, Bong-Seo Kim, and Bok-Ki Min

Korea Electrotechnology Research Institute, Energy Conversion Research Center, Changwon 51543, Republic of Korea

Abstract: In this study, half-Heusler (HH) thermoelectric materials $Nb_{0.8}Hf_{0.2}FeSb_{0.98}Sn_{0.02}$ (p-type) and $Hf_{0.25}Zr_{0.25}Ti_{0.5}NiSn_{0.98}Sb_{0.02}$ (n-type) were synthesized using induction melting and spark plasma sintering. For alloying, a conventional induction melting technique was employed rather than arc melting, for mass production compatibility, and the thermoelectric properties of the materials were analyzed. The maximum dimensionless figures of merit (zT_{max}) were 0.75 and 0.82 for the p- and n-type material at 650 °C and 600 °C, respectively. These materials were then used to fabricate generator modules, wherein two pairs of p- and n-legs without interfacial metal layers were brazed on direct bonded copper (DBC)/Al_2O_3 substrates using a Zr-based alloy. A maximum power of 0.57 W was obtained from the module by applying a temperature gradient of 476 °C, which corresponds to a maximum power density of 1.58 W cm $^{-2}$ when normalized by the area of the material. The maximum electrical conversion efficiency of the module was 3.22% at 476 °C temperature gradient. This value was negatively affected by the non-negligible contact resistivity of the brazed interfaces, which ranged from 6.63×10^{-9} Ω m^2 to 7.54×10^{-9} Ω m^2 at hot-side temperatures of 190 °C and 517 °C, respectively. The low electrical resistivity of the HH materials makes it especially important to develop a brazing technique for ultralow resistance contacts.

(Received August 11 2021; Accepted August 31, 2021)

Keywords: thermoelectric, half-Heusler, module, brazing, contact resistivity

1. Introduction

Thermoelectric technology has been utilized for cooling and power generation because of its salient features, including noiseless operation, small volume, and long-term reliability. Recent interests in eco-friendly power sources are invigorating research in waste heat recovery by thermoelectric generation (TEG). Among the many thermoelectric materials, half-Heusler (HH) materials have attracted attention for mid- to high- temperature applications up to 1,000 K. HH materials possess many merits, including high efficiency, mechanical robustness, low toxicity, and thermal stability [1-6]. *M*NiSn (*M* =Ti, Zr, or Hf) and *R*FeSb (*R* =V, Nb, or Ta) alloys are representative HH materials that have exhibited excellent thermoelectric performances, and a maximum dimensionless figure of merit (zT_{max}) of approximately 1.5 was recently reported for both materials [7,8].

Compared with the abundance of reports on HH material synthesis, reports on module fabrication and characterization are relatively scarce [1,5,6,9-13]. Developing robust and highly conductive metallization for mid-temperature modules is a challenging task that requires a reliable bonding process. The true difficulty stems from the intrinsically high electrical conductivity (σ) of HH materials; the electrical contact resistance (R_c) should be accordingly low to avoid degrading module performance. This is clearly shown in Equation (1) [14]:

$$ZT = (zT)_0\left[\frac{L}{L+2R_c\sigma}\right], \quad (1)$$

where ZT and $(zT)_0$ are the figures of merit for the module and material, respectively, and L is the length of the thermoelectric leg. Making the $R_c\sigma$ term negligibly small is more difficult with HH materials.

Referring to previous reports, different strategies have been employed for bonding HH materials to fabricate modules.

- 주성재 · 김봉서 · 민복기: 책임연구원, 손지희 · 장정인: 연구지원원
**Corresponding Author:*
[Tel: +82-55-280-1627, E-mail: sj_joo@keri.re.kr]

For example, Zillmann *et al*. deposited Au/TiW bilayers on $Hf_{0.5}Zr_{0.5}CoSn_{0.2}Sb_{0.8}$ and $Hf_{0.6}Zr_{0.4}NiSn_{0.98}Sb_{0.02}$ materials as diffusion barriers, which were subsequently sinter-bonded on Ag pads using Ag particles [13]. The contact resistivity was estimated to be 6.2 -10.0 × 10^{-9} Ω m^2 [13]. Yu *et al*. did not use interfacial layers between the HH legs and Cu electrodes. The hot-sides of their HH legs were brazed using a Ag -Cu -Zn alloy in vacuum, and achieved a contact resistivity of 2.0 × 10^{-9} Ω m^2 [5]. Likewise, Nozariasbmarz *et al*. employed direct brazing of $Hf_{0.5}Zr_{0.5}CoSb_{0.8}Sn_{0.2}$ and $Hf_{0.75}Zr_{0.25}NiSn_{0.99}Sb_{0.01}$ on Cu electrodes using a Cu -Ag - based material and reported a remarkable contact resistivity of less than 1 × 10^{-10} Ω m^2 [6]. Xing *et al*. obtained a low contact resistivity of 1.2 × 10^{-9} Ω m^2 using an Ag -Cu -Zn alloy for brazing of $Zr_{0.5}Hf_{0.5}NiSn_{0.97}Sb_{0.03}$ and $Nb_{0.86}Hf_{0.14}$ FeSb. Their careful design of the HH modules resulted in the record power density of 3.1 W cm^{-2} and conversion efficiency of 10.5% [15]. In many cases, high-conductivity alloy metals containing Ag and Cu have been used for brazing.

In this study, $Nb_{0.8}Hf_{0.2}FeSb_{0.98}Sn_{0.02}$ (p-type) and $Hf_{0.25}Zr_{0.25}Ti_{0.5}NiSn_{0.98}Sb_{0.02}$ (n-type) were synthesized, and used to fabricate HH modules. A Zr-based alloy metal containing Ni, Ti, and Cu as minor elements was selected for brazing to test the feasibility of a filler metal that does not contain Ag, a precious metal. Two-pair HH modules were fabricated by direct brazing without diffusion barriers, and the output performance was characterized.

2. Experimental Procedure

Elemental source materials of Hf (99.9%, 3-12 mm pieces, Alfa Aesar), Nb (99.95%, 3.175 mm diameter × 3.175 mm length slug, Alfa Aesar), Fe (99.99%, 3.2 -6.4 mm pieces, Alfa Aesar), Sb (99.999%, 2 mm grains, Kojundo), Zr (99.8%, 3–6 mm lump, Alfa Aesar), Ti (99.99%, 2–10 mm grains, Kojundo), Ni (99.995%, 3.175 -mm -diameter × 3.175 -mm –length slug, Alfa Aesar), and Sn (99.999%, 2–3 mm grains, Kojundo) were used for the synthesis of $Nb_{0.8}Hf_{0.2}FeSb_{0.98}Sn_{0.02}$ and $Hf_{0.25}Zr_{0.25}Ti_{0.5}NiSn_{0.98}Sb_{0.02}$. Raw materials were weighed according to the stoichiometric composition, sealed in a quartz tube in an Ar atmosphere, and then melted completely by conventional RF induction heating equipment. The melted metal was immediately dipped into water for quenching, crushed manually into smaller pieces, and then vacuum-sealed in a quartz tube for a long anneal at 900 ºC. The annealed materials were then ball-milled at 300 RPM (PM-100, Retsch) and sieved to filter out large particles (≥ 45 μm). The fine powders were loaded into a graphite mold (12.7 mm diameter) and spark plasma-sintered (Dr. Sinter, Fuji Electronic Industrial) at 1100 ºC ($Hf_{0.25}Zr_{0.25}Ti_{0.5}NiSn_{0.98}$ $Sb_{0.02}$) or 950 ºC ($Nb_{0.8}Hf_{0.2}FeSb_{0.98}$ $Sn_{0.02}$) under pressure of 65 MPa. The sintered ingots were sawed into various sizes to measure resistivity (ρ), Seebeck coefficient (S), thermal diffusivity (a), and heat capacity (C_p).

The phases in the samples were identified using X-ray diffractometry (XRD, CuKα, X'Pert PRO MPD, Panalytical). The microstructural features were observed using field emission scanning electron microscopy (FE-SEM, S-4800, Hitachi), which was equipped with an energy dispersive X-ray spectroscopy (EDS) system for element mapping and quantitative composition analysis. ρ and S were simultaneously measured using a commercial system (ZEM-3, Ulvac-Riko). A differential scanning calorimeter (DSC 404C, Netzsch) and a laser flash measurement system (LFA-457, Netzsch) were used to measure the C_p and a of the samples, respectively. The density (d) of the samples was measured using the Archimedes method. From these parameters, thermal conductivity (κ) was calculated according to the relation $\kappa = aC_pd$.

The two-pair HH modules were fabricated by brazing HH legs (leg dimensions: 3.0 mm × 3.0 mm × 5.0 mm) on direct bonded copper (DBC)/Al_2O_3 substrates (Cu thickness = 270 μm, area = 1 cm^2) using commercial amorphous alloy foils containing Zr, Ni, Ti, and Cu (thickness = 65 μm) [16]. The heat cycle of brazing was completed in a rapid thermal processing chamber with halogen lamps, where the HH modules were heated at 830 ºC in a N_2 atmosphere for two minutes. Both the hot- and cold- sides of the HH legs were brazed with the same Zr-based alloy. The fabricated modules were characterized using a commercial system (Mini-PEM, Advance Riko, Inc.) that measures the output power and thermoelectric conversion efficiency for small modules up to the highest hot-side temperature of approximately 500 ºC. During the measurement in this study, the hot side of the module was heated up to the highest temperature of 517 ºC, during which the temperature of the water-cooled cold side

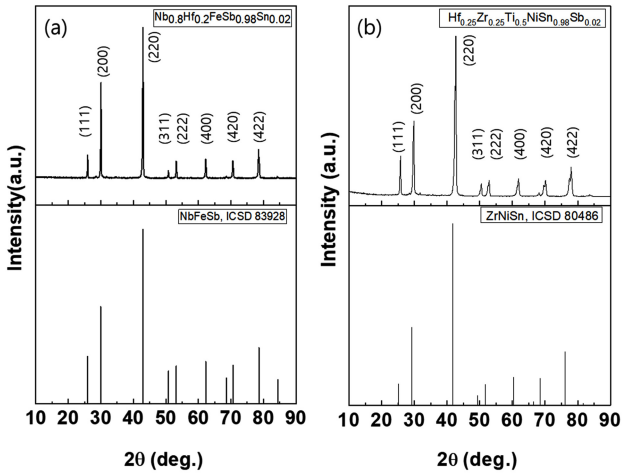

Fig. 1. XRD patterns from the as-sintered $Nb_{0.8}Hf_{0.2}FeSb_{0.98}Sn_{0.02}$ and $Hf_{0.25}Zr_{0.25}Ti_{0.5}NiSn_{0.98}Sb_{0.02}$ samples.

was slightly raised to 41.5 °C through heat conduction.

3. Results and Discussion

3.1 Materials synthesis and thermoelectric performances

Fig. 1 presents the XRD patterns of the sintered $Nb_{0.8}Hf_{0.2}FeSb_{0.98}Sn_{0.02}$ and $Hf_{0.25}Zr_{0.25}Ti_{0.5}NiSn_{0.98}Sb_{0.02}$. All major peaks are clearly identified according to the reference patterns of NbFeSb (ICSD ID: 83928) and ZrNiSn (ICSD ID: 80486), and no other peaks from impurity phases are observable.

Fig. 2 illustrates the thermoelectric properties of the HH materials. In Fig. 2(a), the resistivity values of both materials are in the 10^{-6} Ω m range and increase monotonically with temperature, showing metallic conduction behavior. The absolute values of the Seebeck coefficients also increase with temperature and reach comparable maximum values of 1.68×10^{-4} V K^{-1} and -1.66×10^{-4} V K^{-1} at 700 °C, as illustrated in Fig. 2(b). From the resistivity and Seebeck coefficient, the power factor (*PF*) is calculated from the relation $PF = S^2/\rho$, and the results are illustrated in Fig. 2(c). Overall, the *PF* of $Nb_{0.8}Hf_{0.2}FeSb_{0.98}Sn_{0.02}$ is higher than 4.0×10^{-3} W K^{-2}m^{-1} over the whole temperature range, and PF_{max} is 5.2×10^{-3} W K^{-2}m^{-1} at 300 °C, whereas $Hf_{0.25}Zr_{0.25}Ti_{0.5}NiSn_{0.98}Sb_{0.02}$ has lower PF_{max} of 4.4×10^{-3} W K^{-2}m^{-1} at 400 °C. Consequently, the low resistivity of $Nb_{0.8}Hf_{0.2}FeSb_{0.98}Sn_{0.02}$ produced high *PF*s.

Fig. 2(d) illustrates the thermal conductivity (κ) of both materials. It is observed that $Nb_{0.8}Hf_{0.2}FeSb_{0.98}Sn_{0.02}$ has higher values over the whole temperature range. The κ of $Nb_{0.8}Hf_{0.2}FeSb_{0.98}Sn_{0.02}$ monotonically decreases from 9.1 W K^{-1}m^{-1} at 25°C to 5.4 W K^{-1}m^{-1} at 700 °C, whereas that of

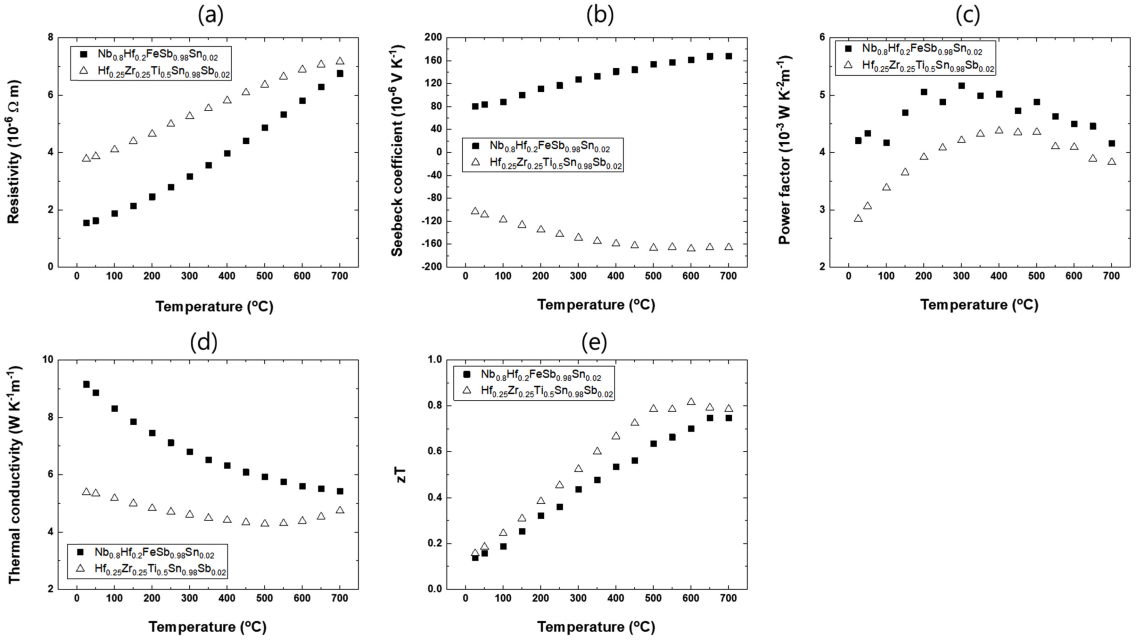

Fig. 2. Thermoelectric properties of the $Nb_{0.8}Hf_{0.2}FeSb_{0.98}Sn_{0.02}$ and $Hf_{0.25}Zr_{0.25}Ti_{0.5}NiSn_{0.98}Sb_{0.02}$: (a) electrical resistivity; (b) Seebeck coefficient; (c) power factor; (d) thermal conductivity; and (e) the dimensionless figure of merit.

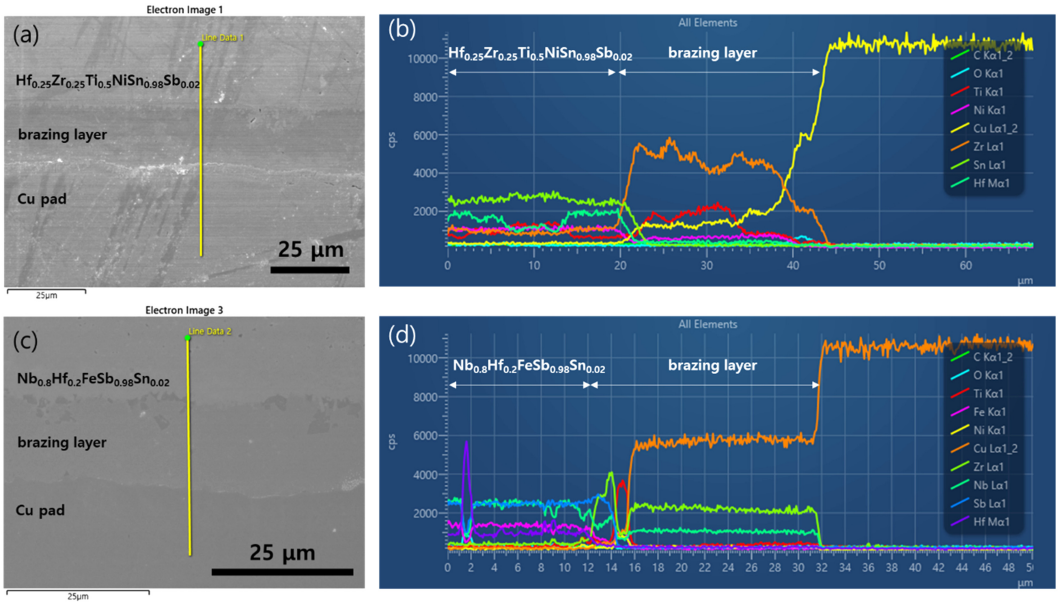

Fig. 3. (a) Cross-sectional SEM image of the brazed interface of $Hf_{0.25}Zr_{0.25}Ti_{0.5}NiSn_{0.98}Sb_{0.02}$ and a Cu pad using a Zr-based filler metal; (b) elemental distribution profiles along the yellow line shown in (a); (c) cross-sectional SEM image of the brazed interface of $Nb_{0.8}Hf_{0.2}FeSb_{0.98}Sn_{0.02}$ and a Cu pad; and (d) elemental distribution profiles along the yellow line shown in (c).

$Hf_{0.25}Zr_{0.25}Ti_{0.5}NiSn_{0.98}Sb_{0.02}$ is relatively constant around approximately 5 W K $^{-1}$m $^{-1}$. From the above parameters, the zT values were calculated using the relation $zT = PF \cdot T/\kappa$, as illustrated in Fig. 2(e), and the zT_{max} of the p- and n-type HH materials was 0.75 and 0.82 at 650 °C and 600 °C, respectively.

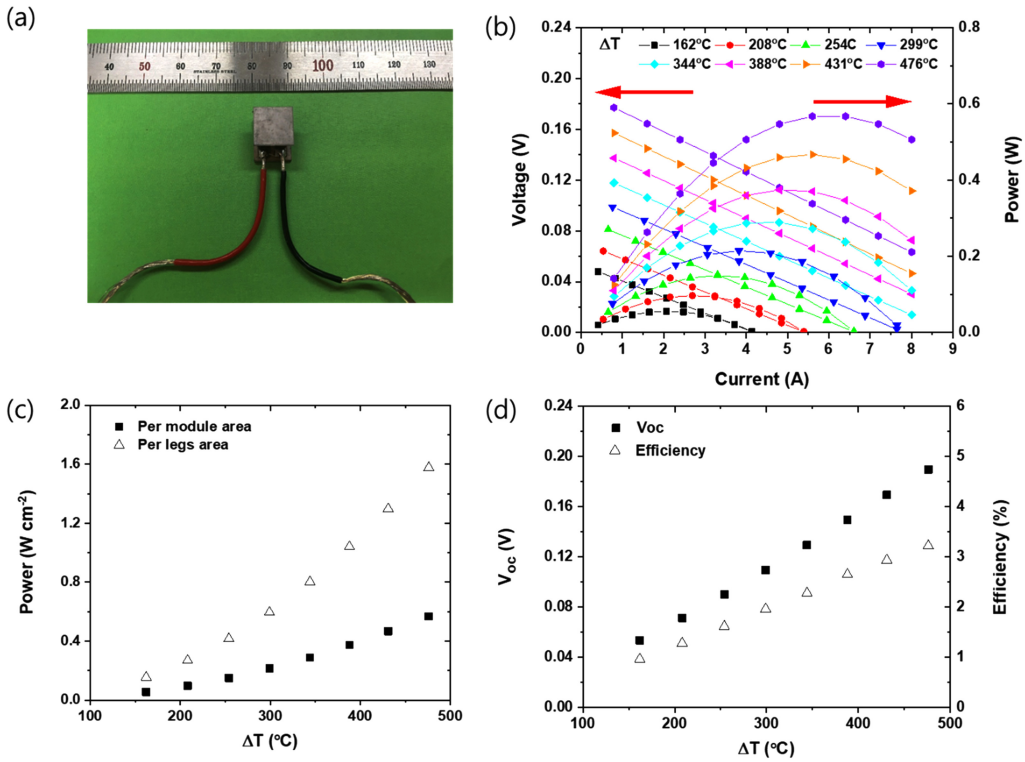

Fig. 4. (a) Photograph of the two-pair HH module; (b) voltage and power versus current of the module under varying ΔT; (c) power density versus ΔT with respect to the legs and the module area; (d) the open-circuit voltage (V_{oc}) and efficiency versus ΔT.

3.2 Module fabrication and characterization

Fig. 3 presents cross-sectional SEM images of the brazed interfaces and corresponding elemental distribution profiles along the yellow vertical lines indicated in Figs. 3(a) and 3 (c). The brazed interfaces of both materials are smooth with no structural imperfections, and the thicknesses of the interfacial layers are approximately 25 and 20 μm for n- and p-type HH, respectively. Fig. 3(b) indicates that the interface between $Hf_{0.25}Zr_{0.25}Ti_{0.5}NiSn_{0.98}Sb_{0.02}$ and the brazing layer is abrupt with an interfacial mixed region with a thickness of approximately 3 μm. The brazing layer is also shown to be mainly composed of Zr, Ti, and Cu. In the case of $Nb_{0.8}Hf_{0.2}FeSb_{0.98}Sn_{0.02}$, Zr and Ti are piled up at the interface with the brazing layer, as confirmed in Fig. 3(d). The main components of the brazing layer were Cu, Zr, and Nb, whose concentrations are quite uniform along the layer. Overall, direct brazing without a diffusion barrier layer resulted in stable bonding and limited reaction at the interfaces. Penetration of Cu into the HH legs was not observed despite the high brazing temperature of 830 ºC.

Fig. 4 illustrates the two-pair HH generator module, and its thermoelectric performance. As illustrated in Fig. 4(b), the output voltage and power increase as the temperature gradient (ΔT) across the module is increased. A maximum power of 0.57 W was obtained at ΔT = 476 ºC and a current of 6.4 A. Fig. 4(c) shows the maximum power density (P_{max}) at each ΔT, which is normalized by the area of the module and the material (legs), respectively. When normalized by the material area, the maximum power density of the module was 1.58 W cm $^{-2}$ at ΔT = 476 ºC. The open-circuit voltage (V_{oc}) increased linearly, up to 0.19 V, with ΔT, as illustrated in Fig. 4(d). The maximum conversion efficiency of the two-pair module was estimated to be 3.22% at ΔT = 476 ºC.

Compared with the results of previous reports by other groups (Table 1), the overall performance of our HH modules is relatively lower. The primary reason for this is the lower ΔT in this study. We also believe that the material properties should be further improved. In addition, contact resistance plays a critical role in deteriorating the ideal performance of the modules, as shown in Equation (1). Accordingly, the contact resistivity of the brazed interfaces was estimated based on the output characteristics of the HH module.

First, the internal resistance of the module (R_{int}) was estimated from the voltage -current relation in Fig. 4(b),

Table 1. Performance of HH generator modules reported in recent representative studies

Material	Module area/Number of p-n pairs	Maximum power density	Maximum efficiency	Contact resistivity (Ω m^2)	Reference
$Zr_{0.4}Hf_{0.6}NiSn_{0.98}Sb_{0.02}$ $Zr_{0.5}Hf_{0.5}CoSb_{0.8}Sn_{0.2}$	16 × 16 mm^2, seven pairs	1.09 W cm^{-2} @ ΔT=527 ºC (module area)	5 %	-	[10]
$Zr_{0.4}Hf_{0.6}NiSn_{0.98}Sb_{0.02}$ $Zr_{0.5}Hf_{0.5}CoSb_{0.8}Sn_{0.2}$	13 × 9 mm^2, two pairs	1.9 W cm^{-2} @ ΔT=400 ºC (legs area)	-	$6.2 \times 10^{-9} \sim 1.0 \times 10^{-8}$	[13]
ZrNiSn-based alloy $FeNb_{0.88}Hf_{0.12}Sb$	20 × 20 mm^2, eight pairs	2.2 W cm^{-2} @ ΔT=655 ºC (module area)	6.2 %	2×10^{-9}	[11]
$Hf_{0.75}Zr_{0.25}NiSn_{0.99}Sb_{0.01}$ $Hf_{0.5}Zr_{0.5}CoSb_{0.8}Sn_{0.2}$	unicouple (leg dimension: 2.5 × 2.5 × 2.0 mm^3)	8.9 W cm^{-2} @ ΔT=678 ºC (legs area)	8.9%	1×10^{-10}	[12]
$Zr_{0.5}Hf_{0.5}NiSn_{0.985}Sb_{0.015}$ $Zr_{0.5}Hf_{0.5}CoSb_{0.8}Sn_{0.2}$	20 × 20 mm^2, eight pairs	2.33 W cm^{-2} @ ΔT=655 ºC (module area)	9.6%	3.3×10^{-9} (n-HH/Cu) 2.8×10^{-9} (p-HH/Cu)	[1]
$Hf_{0.5}Zr_{0.5}NiSn_{0.98}Sb_{0.02}$ $Nb_{0.64}Ta_{0.16}Ti_{0.2}FeSb$	20 × 20 mm^2, eight pairs	2.11 W cm^{-2} @ ΔT=655 ºC (module area)	8.3%	2×10^{-9}	[5]
$Hf_{0.75}Zr_{0.25}NiSn_{0.99}Sb_{0.01}$ $Hf_{0.5}Zr_{0.5}CoSb_{0.8}Sn_{0.2}$	six unicouples (leg dimension: 2.3 × 2.3 × 1.9 mm^3)	11.5 W cm^{-2} @ ΔT=670 ºC (legs area)	9.5%	$< 1 \times 10^{-10}$	[6]

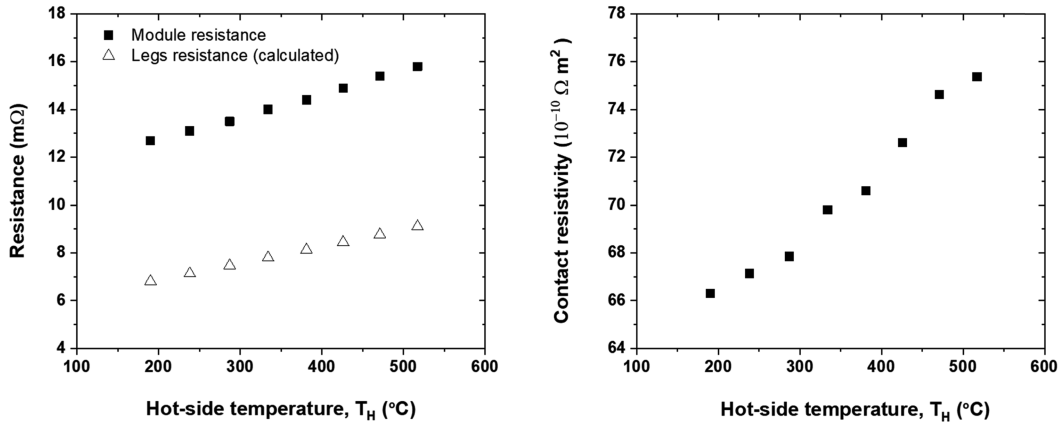

Fig. 5. (a) Module resistance (measured) and leg resistance (calculated) versus hot-side temperature T_H; (b) calculated contact resistivity versus hot-side temperature T_H.

which is plotted in Fig. 5(a) as a function of the hot-side temperature, T_H. The R_{int} of our module was approximately 12.7 mΩ at T_H = 190 °C and increased linearly up to 15.8 mΩ at 517 °C. Since R_{int} is composed of the resistances of the thermoelectric materials (R_{TE}), contacts ($R_{contact}$), and Cu pads (R_{pad}), if we ignore the negligible contribution from R_{pad}, $R_{contact}$ can be estimated using the following relation:

$$R_{int} = R_{TE} + R_{contact}. \quad (2)$$

The R_{TE} is easily calculated from the resistivity data of the HH materials in Fig. 2(a) by assuming that the temperature gradient is constant along the HH legs; the final result is plotted in Fig. 5(a). It is noted that the R_{int} is approximately twice as high as R_{TE}, showing that the magnitude of $R_{contact}$ is comparable to that of R_{TE}.

Normalizing $R_{contact}$ by the area of the contacts and the number of interfaces leads to a contact resistivity of 6.63×10^{-9} Ω m^2 at T_H = 190 °C, which increases up to of 7.54×10^{-9} Ω m^2 at 517 °C as illustrated in Fig. 5(b). This estimation is based on a simple assumption that the contact resistivity values for p- and n-type HH materials are equal. When one compares the magnitudes of contact resistivity, the Zr-based filler metal in this study produces somewhat higher values than the cases using Ag -Cu -Zn, which were in the range 1.2 -2.0 × 10^{-9} Ω m^2 [5,15]. This discrepancy may partly arise from the intrinsically higher resistivity of Zr (4.21×10^{-7} Ω m at 20 °C) than Ag (1.59×10^{-8} Ω m at 20 °C) and Cu (1.68×10^{-8} Ω m at 20 °C). Nevertheless, further optimization of the brazing process, including soaking temperature and time, is expected to lower the contact resistivity. Reducing the contact resistivity below 1×10^{-9} Ω m^2 would be required to maximize the conversion efficiency and output power of our HH modules.

4. Conclusions

In this study, HH materials were fabricated and brazed to make two-pair thermoelectric generator modules. $Nb_{0.8}Hf_{0.2}FeSb_{0.98}Sn_{0.02}$ and $Hf_{0.25}Zr_{0.25}Ti_{0.5}NiSn_{0.98}Sb_{0.02}$ were synthesized by induction melting and spark plasma sintering, and the zT_{max} values of 0.75 and 0.82 were obtained for the p- and n-type material, respectively. For metallization of the HH legs, direct brazing without diffusion barrier layers was implemented using a Zr-based amorphous alloy. Smooth and abrupt interfaces were produced with a contact resistivity of about 6.63×10^{-9} Ω m^2 at T_H = 190 °C. The maximum power output of the two-pair HH modules was 0.57 W at ΔT = 476 °C, which corresponds to a maximum conversion efficiency of 3.22%. Establishing an optimized brazing process is crucial to increase the module performance.

Acknowledgment

This research was supported by Korea Electrotechnology Research Institute(KERI) Primary Research program through the National Research Council of Science & Technology (NST) funded by the Ministry of Science and ICT (MSIT)

(no. 21A01011).

Conflicts of Interest

All authors declare no conflicts of interest.

REFERENCES

1. Y. Xing, R. Liu, J. Liao, Q. Zhang, X. Xia, C. Wang, H. Huang, J. Chu, M. Gu, T. Zhu, C. Zhu, F. Xu, D. Yao, Y. Zeng, S. Bai, C. Uher, and L. Chen, *Energy Environ. Sci*. **12**, 3390 (2019).
2. G. Rogl, A. Grytsiv, M. Gürth, A. Tavassoli, C. Ebner, A. Wünschek, S. Puchegger, V. Soprunyuk, W. Schranz, E. Bauer, H. Müller, M. Zehetbauer, and P. Rogl, *Acta Mater*. **107**, 178 (2016).
3. W. Silpawilawan, K. Kurosaki, Y. Ohishi, H. Muta, and S. Yamanaka, *J. Mater. Chem. C* **5**, 6677 (2017).
4. A. Tavassoli, F. Failamani, A. Grytsiv, G. Rogl, P. Heinrich, H. Müller, E. Bauer, M. Zehetbauer, and P. Rogl, *Acta Mater*. **135**, 263 (2017).
5. J. Yu, Y. Xing, C. Hu, Z. Huang, Q. Qiu, C. Wang, K. Xia, Z. Wang, S. Bai, X. Zhao, L. Chen, and T. Zhu, *Adv. Energy Mater*. **10**, 2000888 (2020).
6. A. Nozariasbmarz, U. Saparamadu, W. Liu, H.B. Kang, C. Dettor, H. Zhu, B. Poudel, and S. Priya, *J. Power Sources* **493**, 229695 (2021).
7. G. Rogl, P. Sauerschnig, Z. Rykavets, V.V. Romaka, P. Heinrich, B. Hinterleitner, A. Grytsiv, E. Bauer, and P. Rogl, *Acta Mater*. **131**, 336 (2017).
8. C. Fu, S. Bai, Y. Liu, Y. Tang, L. Chen, X. Zhao, and T. Zhu, *Nat. Commun*. **6**, 8144 (2015).
9. S.J. Poon, D. Wu, S. Zhu, W. Xie, T.M. Tritt, P. Thomas, and R. Venkatasubramanian, *J. Mater. Res*. **26**, 2795 (2011).
10. K. Bartholomé, B. Balke, D. Zuckermann, M. Köhne, M. Müller, K. Tarantik, and J. König, *J. Electron. Mater*. **43**, 1775 (2014).
11. C. Fu, S. Bai, Y. Liu, Y. Tang, L. Chen, X. Zhao, and T. Zhu, *Nat. Commun*. **6**, 1 (2015).
12. G. Joshi and B. Poudel, *J. Electron. Mater*. **45**, 6047 (2016).
13. D. Zillmann, D. Metz, B. Matheis, A. Dietzel, A. Waag,
14. and E. Peiner, *J. Electron. Mater*. **48**, 5363 (2019).
15. L.I. Anatychuk and O.J. Luste, *Proc. 15th International Conference on Thermoelectrics*, 279, International Thermoelectric Society, Pasadena, USA (1996).
16. Y. Xing, R. Liu, J. Liao, C. Wang, Q. Zhang, Q. Song, X. Xia, T. Zhu, S. Bai, and L. Chen, *Joule* **4**, 2475 (2020).
17. ECO FM Co., Ltd.www.ecofm.co.kr.